García-Hernando, N., Venegas, M. & de Vega, M. (2019). Experimental performance comparison of three flat sheet membranes operating in an adiabatic microchannel absorber. *Applied Thermal Engineering*, vol. 152, pp. 835–843.

DOI: 10.1016/j.applthermaleng.2019.02.129

Experimental performance comparison of three flat sheet membranes operating in an adiabatic microchannel absorber

N. García-Hernando [a], M. Venegas [a,b], M. de Vega [a*].

[a] ISE, Thermal and Fluids Engineering Department, Universidad Carlos III de Madrid, Avda. Universidad 30, 28911 Leganés, Madrid, Spain

[b] GTADS, Thermal and Fluids Engineering Department, Universidad Carlos III de Madrid, Avda. Universidad 30, 28911 Leganés, Madrid, Spain

Abstract

A microchannel absorber working adiabatically with the H_2O-LiBr pair was tested experimentally using three different nanofibrous flat membranes separating the vapour from the solution. Pore diameters of the membranes were 1 and 0.45 μm, and thicknesses vary from 25 to 175μm. The experimental absorption rates ranged from 1.5 10^{-3} to 2.6 10^{-3} kg/m^{2}s varying linearly with the solution mass flow rate circulating through the channels. The reduction in pore diameter from 1 μm to 0.45 μm induced the need for higher pressure potential or solution mass flow rate to obtain similar performance. Relationships between changes in diameter pore and membrane thickness from previous models were used to quantify the effect of these membranes characteristics on the absorption ratio. The analytical results compared well with our experiments. In the present design, the solution film thickness was 150 μm and the solution mass transfer resistance dominated the process. The experimental overall resistances, compared with calculated values from correlations used in previous models, showed differences below 30%.

Keywords: Cooling absorption; microchannel absorber; membranes; H_2O-LiBr.

Nomenclature

A	area (m^2)
D	diffusion coefficient (m^2 s^{-1})

* Corresponding author.
E-mail address: mdevega@ing.uc3m.es (M. de Vega).

D_h hydraulic diameter (m)

d_p membrane pore diameter (m)

e height or thickness (m)

J absorption rate (kg m^{-2} s^{-1})

k_s solution mass transfer coefficient (m. s^{-1})

l width (m)

$\dot{m}$ mass flow rate (kg s^{-1})

M molecular weight (kg $kmol^{-1}$)

P pressure (kPa)

R mass transfer resistance (kg^{-1} Pa m^2 s)

Re Reynolds number

Sc Schmidt number

Sh Sherwood number

R_u universal gases constant

T temperature (ºC)

Greek symbols

ε porosity

μ viscosity (N.s m^{-2})

ρ density (kg. m^{-3})

τ tortuosity

Subscripts

m membrane

OV overall

s solution

sat saturation

v vapour

va vapour absorbed

w wall-water

1. Introduction

Currently, electricity-driven vapour-compression systems, mainly based on fossil fuels, dominate the air-conditioning market. Unfortunately, this seems not very compatible with a clean energy sustainable world. There is a need to encourage the use of technologies based on renewable energy sources, such as absorption cooling chillers, fed by residual or renewable thermal energy, i.e. solar energy, to avoid indirect CO_2 emissions attributed to the refrigeration systems. In addition, a reduction in the volume of the chillers is required in order to obtain competitive absorption systems, in the low-medium capacity range.

In the past, tests of new configurations for the main components in the absorption chiller, absorber and generator, tried to improve their performance by means of sprays, bubbles or plate heat exchangers. Another option is the use of microporous membranes separating the refrigerant vapour from the solution in the absorber and the desorber. In this way, a large interfacial area is available for mass transfer between both phases. Some configurations using hollow fibre and flat membranes with NH_3-H_2O and H_2O-LiBr fluid pairs, have shown promising results. In the present work, the experimental performance of flat membranes, in the case of the H_2O-LiBr solution flowing in confined rectangular microchannels is considered. The main parts of such a system are presented in Fig. 1. The solution flows through the microchannels and is separated from the vapour by the membrane. In the membrane, many small diameter pores avoid mixing between vapour and solution, while allow the gas and solution to be in contact. The gaseous fluid (in the present case water vapour) passes the membrane and is absorbed by the H_2O-LiBr solution flowing inside the constrained flow passages. In the figure, a perforated stainless steel plate is also represented. It is usually used as support to avoid deformation of the thin membrane. The figure represents an adiabatic configuration, which will be the case in the present study. For the cooled case, water circulates through similar channels separated from the solution by a metallic wall and extracts the heat of absorption.

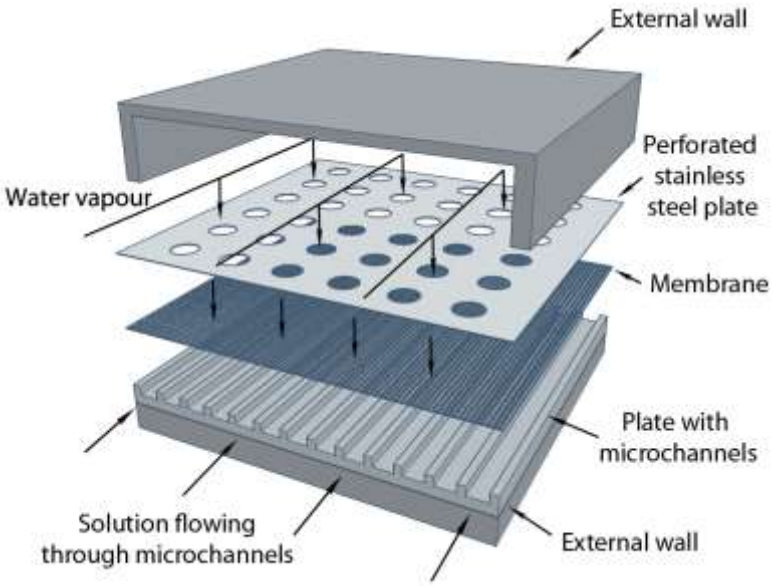

Fig. 1. Membrane based adiabatic microchannel absorber configuration.

Ali and Schwerdt [1] and Ali [2] presented experimental and theoretical studies of a flat membrane-based absorber using the H_2O-LiBr solution. Different PTFE (Polytetrafluoroethylene) membranes, with pore diameters of 0.2, 0.22 and 0.45 μm and variable thicknesses (from 60 to 175 μm), were tested in a test cell, 4 mm in depth, without cooling water. Results indicated that, for comparable pore sizes, the supported thin membranes showed a larger vapour flux than the unsupported thick membranes. The measured absorption rates were on the order of 1.2 10^{-3} kg/m^{2}s, which is nearly half the value found in conventional absorbers. The absorption rate was not affected by changes in the solution mass flow rate, which varied in a range from 2 to 14 kg/h. The authors argued that the membrane mass transfer resistance controlled the process. In their experiments, the effect of the variation of the operating conditions was within the uncertainty of the results. The sensitivity of the absorption rate to the main membrane properties (pore diameter, thickness and porosity) was analysed with an analytical model, which agreed with these experimental results. It was concluded that a large pore diameter in combination with a porosity of 80% almost doubled the vapour flux compared to a porosity of 60%. In order to guarantee a sufficient strength to support the membrane inside the absorber and, with the objective of reaching high vapour fluxes, the authors considered an appropriate porosity one that was between 70 to 80%.

Later, Yu et al. [3] presented a 2D numerical simulation and studied the effects on the absorption rate of the solution properties (film thickness, velocity and

concentration), the main membrane characteristics (pore diameter, thickness and porosity) and the temperature of the cooling water. They compared the relative importance in the overall mass transfer of the membrane resistance and the diffusion resistance into the solution film. They demonstrated that the main parameters for a high absorption rate are the solution film thickness and the solution velocity. Their numerical investigation showed that a larger absorption rate, comparing to conventional absorbers, can be achieved for solution thicknesses in the range of 50 to 100 μm. They finally considered the effect of the membrane roughness that can increase the absorption rate by 15% compared to a smooth membrane surface. Bigham et al. [4] developed a numerical study that showed that the inclusion of micro corrugations in the solution channel enhanced the mass transfer. In this case, the authors used a membrane of 20 μm thickness, 60% porosity and 1 μm pore size. The solution channels height was 0.5 mm.

Asfand et al. [5] by means of a CFD simulation studied a membrane-based water cooled absorber. The authors used a plate-and-frame configuration and the H_2O-LiBr solution. In this case, the membrane had a thickness of 60 μm, a pore size of 0.45 μm and a porosity equal to 75%. The solution channel thickness ranged between 0.25 and 2 mm. In another study, Asfand et al. [6] used a quaternary and a ternary mixture, based on water as refrigerant, and numerically evaluated the performance of the plate and frame membrane-based absorber. The authors modified the membrane and solution film characteristics, using 85% porosity, 40 μm thickness, 1 μm pore diameter and 0.5 mm solution film thickness. Again, with the H_2O-LiBr solution, Asfand et al. [7] numerically studied the effect in the absorption rate of the solution thickness (with values of 0.1, 0.25, 0.5 and 1 mm) and the membrane properties on a water-cooled absorber cell, 200 mm long and 200 mm wide. The analysis of membrane properties concerned porosity (varying between 50 and 85%), thickness (ranging between 20 to 100 μm) and pore diameter (changing from 0.25 to 3 μm). Results showed that the membrane characteristics affect in different ways depending on the solution channel thickness.

The model of Venegas et al. [8,9] was used to stablish the relative importance of the main membrane parameters such as pore diameter, porosity and thickness (which were varied in ranges of 0.3-1.5 μm, 50-90% and 50-210 μm) in the design of a microchannel absorber. This model was used later in Venegas et al. [10] to compare two different configurations of microchannel membrane-based absorbers: in one case using

cooling water to extract the absorption heat (non-adiabatic) and, in the other one, considering a novel adiabatic configuration. The analysis dealt with a membrane of 80% porosity, 1 μm pore diameter and 60 μm thickness. Comparison of both configurations provided average absorption rates of $2.3.10^{-3}$ and $3.3.10^{-3}$ kg/m^{2}s in the adiabatic and non-adiabatic cases. This difference was attributed to the effect of the cooling water in the non-adiabatic absorber, that provides a continuous subcooling of the solution. It was concluded also that the adiabatic configuration was more sensitive to the inlet solution mass flow rate.

Isfahani and Moghaddam [11] and Isfahani et al. [12] presented permeability studies in nanofibrous membranes, leading to a successful implementation of a 1 μm pore size and 80% porosity membrane in a water cooled microchannel absorber. They experimentally compared the absorption rate using this membrane in two different geometries of the solution channels: 100 and 160 μm thickness, both of 1 mm width and 38 mm length. They used a supporting plate with an open area of 51%. The authors demonstrated that a decrease of the solution channel height enhances the absorption rate. They also obtained a linear dependence of the absorption rate with the pressure driving potential and of the absorption coefficient with the solution mass flow rate (which was varied from 0.8 to 2.3 kg/h). The absorption rate obtained with the 160 μm in height channel was higher than the one obtained in conventional falling film absorbers. It was also higher than the value reported by Ali and Shwerdt [1] in their plate absorber. Later, Isfahani et al. [13] employed micro protrusions on the solution channel wall to enhance the absorption rate.

Schwerdt [14] developed an absorption module employing flat sheet membranes. Their selection, after characterization of several membranes, consisted on a 0.45 μm pore size and 80% porosity membrane. They obtained absorption rates of 2.25 kg/m^{2}h at pressure potentials of 0.9kPa.

To the author´s knowledge, and according to the literature review, while several models of plate-and-frame or microchannel membrane-based absorbers and the H_2O-LiBr pair have studied the effect on the absorption rate of the membrane characteristics and the operating conditions, very few experimental works have been performed to date. In the present study, the comparison of the absorption rate experimentally measured in an adiabatic absorber working with three different flat membranes is presented. This comparison has not been previously reported for the case of an adiabatic microchannel

absorber. The effect of the different pore diameters, thicknesses and porosities of the membranes on the absorber performance is evaluated at different mass flow rates and pressure potentials, using the same experimental test rig presented in García-Hernando et al. [15]. These novel results are used to evaluate previous theoretical studies. Moreover, the experimental mass transfer resistances are compared with those predicted by correlations used in previous models developed by Ali [2] and Venegas et al. [10] for adiabatic membrane-based microchannel absorbers.

2. Experimental setup

The membranes tested in the microchannel absorber are three different flat sheet PTFE commercially available membranes. PTFE is an hydrophobic polymer, that is inexpensive, thermally stable and chemically resistant (Wang and Chung [16]).

Porous membranes are defined by the microstructure of the pores. This structure for the three tested membranes is shown in Fig. 2.

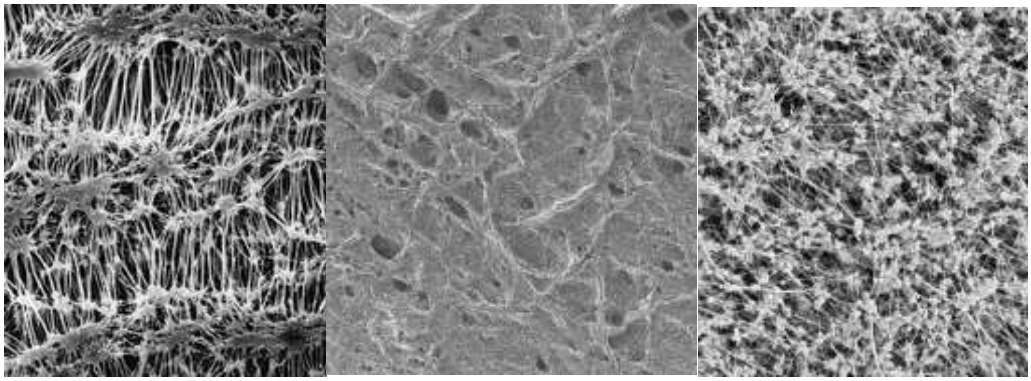

FALP29325 PTU0453001 PTFE0453005

Fig. 2. Membranes compared in the experimental tests (extracted from [17,18,19]).

Pore size and porosity are primary factors affecting mass transfer. Thickness will also contribute to define the travel distance through the pore, and therefore the mass transfer performance. Thus, membranes with large pores and high porosity, low thickness and small tortuosity provide higher vapour transport (Wang and Chung [16], Hong et al. [20]). Nevertheless, there is a limitation concerning mechanical strength that makes the need to have, in some applications, higher thickness or an additional plate support. The main characteristics of each membrane tested relating to these properties are listed in Table 1.

Table 1. Data of the tested membranes (extracted from [17,18,19]).

Parameter	FALP29325 (MEM 1)	PTU0453001 (MEM 2)	PTFE0453005 (MEM 3)
Polypropylene supporting layer	Yes	No	Yes
Thickness, e_m (μm)	175	25-51	76-127
Porosity (%)	85	~90	~90
Pore diameter, d_p (μm)	1	0.45	0.45

The designed adiabatic absorber consisted of a plate-and-frame module in which the solution circulates confined in micro-channels separated from the vapour by the hydrophobic membrane as shown in the schematic layout in Fig. 3.

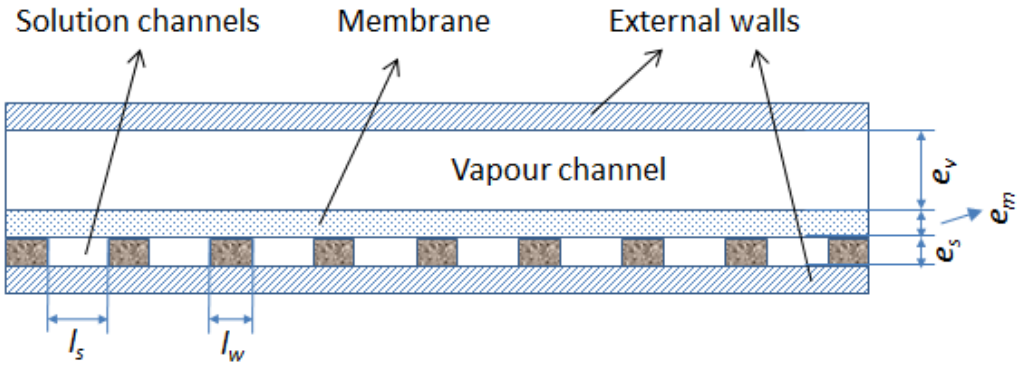

Fig. 3. Scheme of the absorber configuration.

There were 50 microchannels machined in a stainless steel plate, shown in Fig. 4. The channel wall thickness l_w is 0.75 mm. In the present case, as the absorber worked adiabatically, only solution and vapour channels were used. The vapour channel was 5 mm height (e_v) while the solution thickness (e_s), given by the solution channel height was 150μm. The width of the solution channel, l_s, was 3mm. The total length of the channels in the absorber was 5.8 cm.

Fig. 4. Microchannels mechanized in the stainless steel plate.

The membrane was placed above the solution channels. The solution was fed into the microchannel, and was constrained by the hydrophobic flat sheet membrane. The mass transfer is governed by the vapour partial pressure difference across the both sides of the membrane: a higher pressure in the vapour side (*Pv*) than the vapour partial pressure in the solution, P_s, promotes the absorption of the water vapour across the membrane. This pressure potential will be defined as $\Delta P = P_v - P_s$, where P_s is the water vapour pressure, at the measured temperature and concentration of the solution. In the present design, an additional thin perforated stainless steel plate (Fig. 5) was used to support the membrane, and provided the needed rigidity.

Fig. 5. Perforated stainless steel supporting plate, 1.5 mm thick, with holes of 3.2 mm diameter.

Fig. 6 shows the whole absorber assembly. The vapour side has a transparent window to allow for visual verification that no condensation occurs or that no liquid solution traverses the membrane.

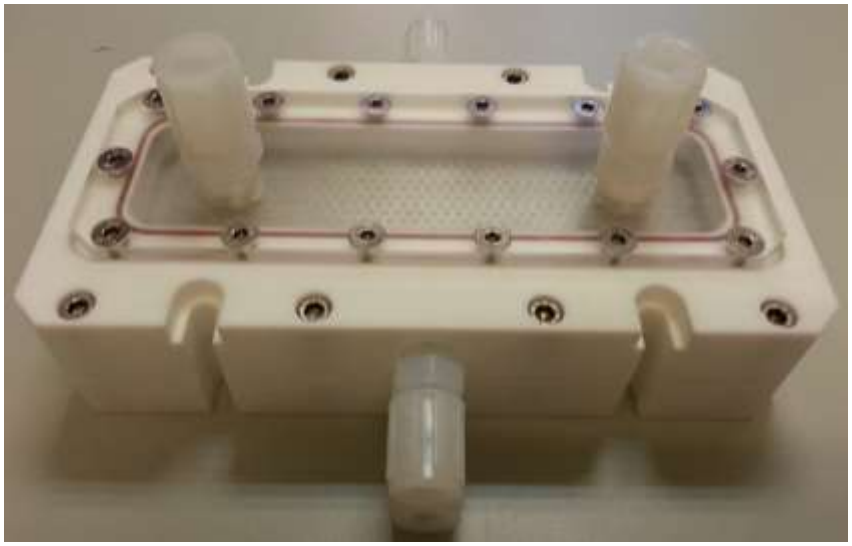

Fig. 6. Photograph of the absorber tested.

The absorption measurements were carried out using the experimental set-up schematized in Fig. 7 and shown in Fig. 8. The main components were described in García-Hernando et al. [15]. It consisted of a vapour generation system, 2 solution vessels, a solution pump and the necessary instrumentation. All the connections were made of stainless steel. Also inert polymers were used to avoid corrosion. From the feeding solution tank, the solution, with a previously defined concentration circulated to the absorber. At the exit of the absorber, another tank recovered the diluted solution. A magnetic pump type assured the solution circulation. A variable frequency driver controlled the solution flow rate. The vapour was generated in a third tank. The vacuum

was assured by a Vacuubrand PC 3001 vacuum pump.

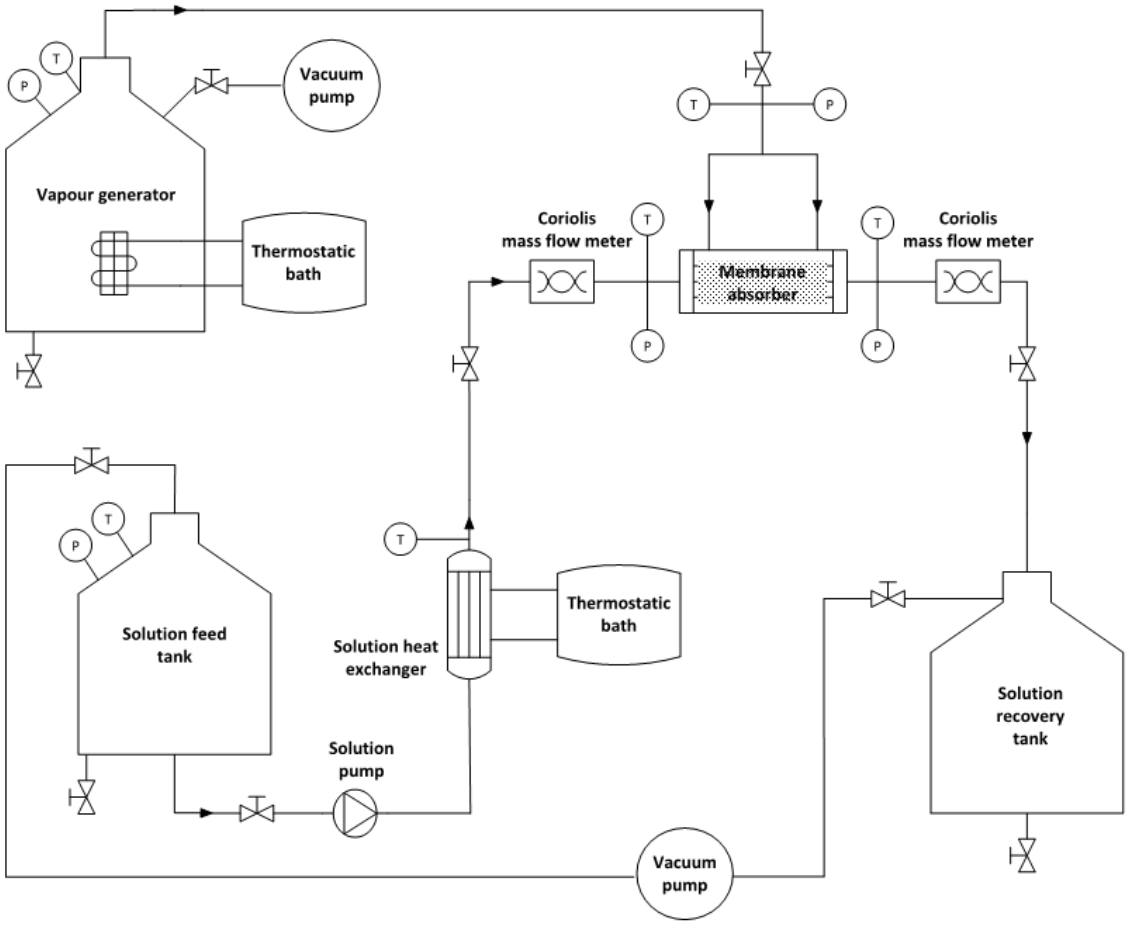

Fig. 7. Scheme of experimental loop.

The experimental procedure was the same for all the experiments. The solution tank was first charged with the solution at the initial concentration. The test started by filling the lines with the solution pump, and once the installation was filled, the valve connecting the vapour generator to the absorber was opened. Temperatures, pressures and mass flow rates were monitored in order to verify steady state conditions. Also a visual inspection through the transparent plate of the absorber allowed to control possible malfunctioning.

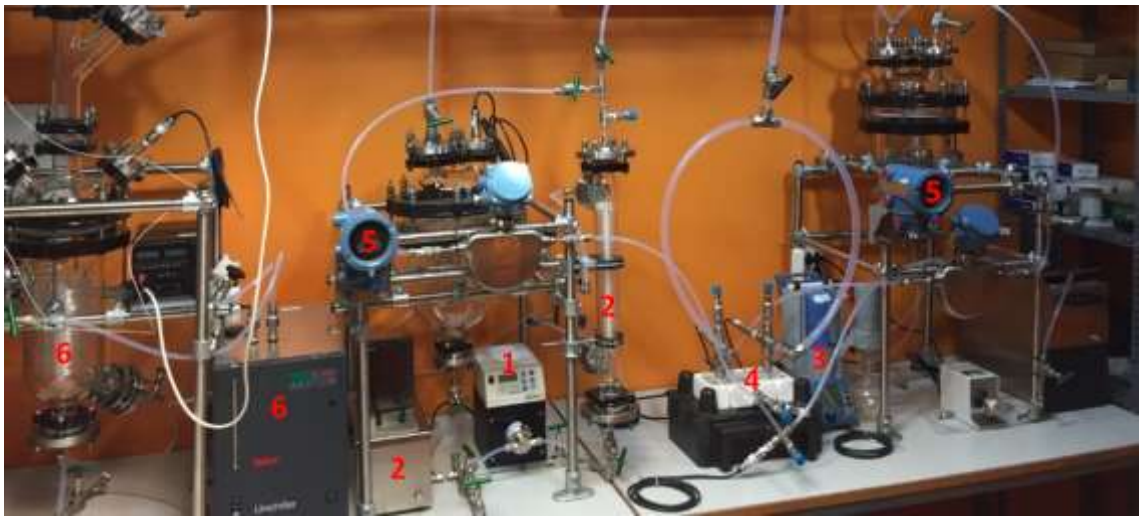

Fig. 8. Photograph of the experimental set-up. 1-solution pump, 2-heat exchanger, 3-Vacuubrand PC 3001, 4-microchannel absorber, 5-flowmeters, 6-vapour generation vessel.

The instrumentation included flowmeters, pressure transducers and thermoresistances. Two Micromotion™ coriolis flowmeters (CFMS010M) measured mass flow rate and density of the solution. The Coriolis flowmeter measured the mass flow rate of the solution at the inlet within a range of 0.002-110 kg/h and an uncertainty of ± 0.1%. Density was measured in a range of 0 to 5000kg/m^3 with an uncertainty of ± 0.5 kg/m^3. Temperature was measured by PT100 thermoresistances (OMEGA series PR-17) with an uncertainty calculated as ± (0.15+0.002*T) ºC. OMEGA PX409-005AI-EH transducers were used for the measurement of the absolute pressure of the vapour and the solution, within a range of 0-5 psi, and an uncertainty of ± 0.025 psi.

The uncertainties obtained according to Taylor and Kuyatt [21] for the main variables are listed in Table 2.

Table 2. Variables uncertainties.

Variable	Uncertainty
Pressure potential, P_v - P_s	1.2%
Solution mass flow rate, $\dot{m}_s$	0.12%
Absorption rate, J	1.7%
Overall mass transfer resistance, R_{OV}	2.2%
Membrane mass transfer resistance, R_m	0.05%
Solution mass transfer resistance, R_s	3%

The three different membranes were tested at the experimental conditions summarized in Table 3.

Table 3. Experimental range of the measured variables.

Parameter	FALP29325 (MEM1)	PTU0453001 (MEM2)	PTFE0453005 (MEM3)
Pressure potential (kPa)	1.4 – 2.94	2.07 – 1.54	3.4 – 3.8
Solution mass flow rate (kg/h)	0.22 – 0.5	0.7 – 1	0.5 – 0.9
Solution concentration [%]	58.6	60	58.2
Solution inlet temperature (ºC)	26 – 28	26 – 28	26 – 28

3. Results and discussion

Fig.9 shows the values of the absorption rate across the membrane into the LiBr aqueous solution, for the three membranes.

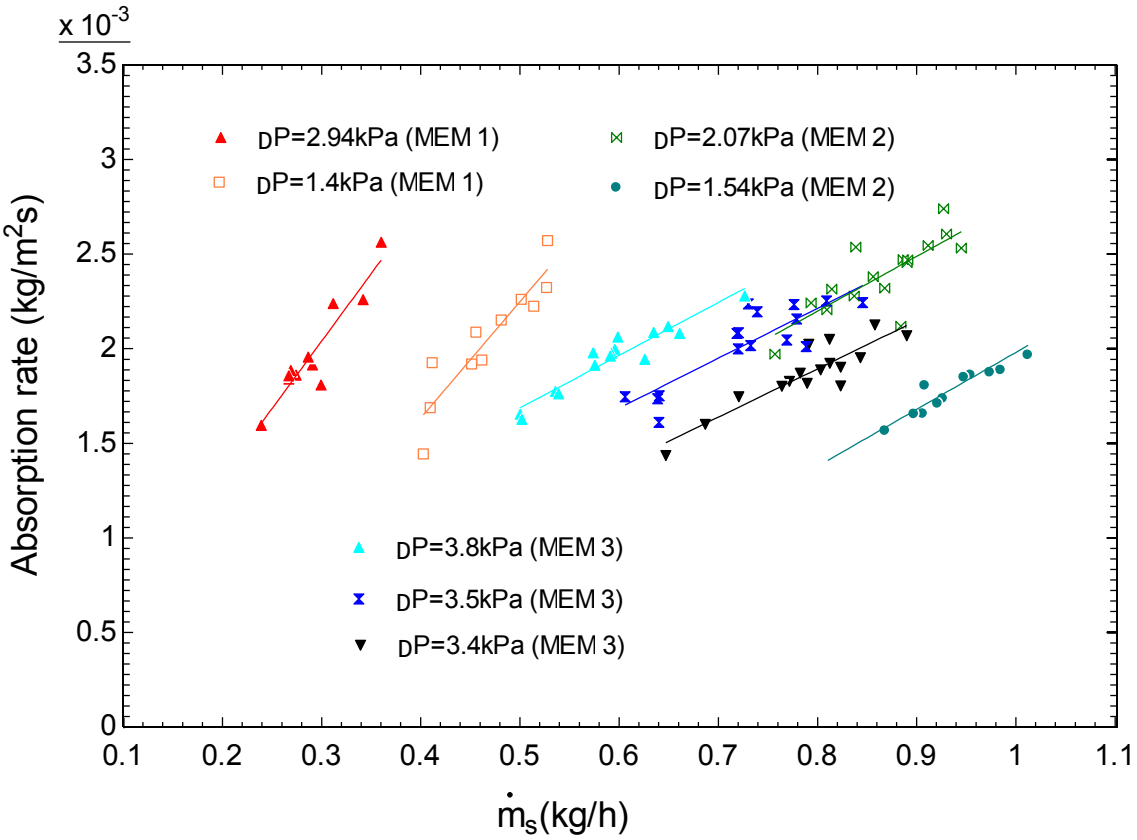

Fig. 9. Measured absorption rates for the three tested membranes at different solution mass flow rates.

The absorption rate (J) was obtained from the measured mass flow rate of vapour absorbed and the contact area (A). This area corresponds to the area of the circular orifices, 3.2 mm in diameter, shaped in the supporting plate (Fig. 5).

$$J = \dot{m}_{va}/_{A} \quad (1)$$

The absorption rate ranges from $1.5.10^{-3}$ to $2.6.10^{-3}$ kg/m^{2}s. The vapour absorbed is lower than in the experiments of Isfahani et al. [12]. This is mainly due to the fact that in the present configuration the absorber is adiabatic. This difference between the adiabatic and non-adiabatic configurations was already remarked and the values experimentally obtained now are in the order of the ones predicted in Venegas et al. [10]. The cooling of the solution during the absorption process can reduce the water pressure of the solution, increasing then the pressure potential, and consequently the absorption rate.

For a given membrane and experimental conditions, the absorption rate increases with the solution mass flow rate. This result is consistent with the previous models of Asfand et al. [7], Venegas et al. [9] and the experimental results of Isfahani et al. [12]. The mass rate of vapour absorbed, according to the mass balance in the absorber, is theoretically proportional to the solution mass flow rate. This could explain the linear relationship between J and the solution mass flow rate. In Asfand et al. [7] and Isfahani et al. [12], an increase with mass flow rate of J is also shown. In those works, the range of change of the solution mass flow rate was larger than in our case, presenting only an approximate linear behavior if the solution mass flow rate changes in a narrower range, as in the present case (0.2 kg/h to 1.1 kg/h). The rate of increase is higher for the higher pore diameter: 0.0065 kg/m^{2}s per kg/h of solution in the 1 μm pore diameter case and 0.00256 kg/m^{2}s per kg/h of solution for a pore diameter of 0.45 μm.

The experiments of Isfahani et al. [12], in their cooled absorber with the 1 μm pore diameter membrane and 160 μm channel, showed an increase with mass flow rate in the order of 0.002 kg/m^{2}s per kg/h of solution which is lower than the one in our case. This is in agreement with Venegas et al. [10] where the simulated adiabatic case was more sensitive to the mass flow rate than the non-adiabatic one.

For similar pressure potentials a reduction in the pore diameter from 1 μm to 0.45 μm implies that the solution mass flow rate must double to obtain similar absorption rates. On the other hand, the membrane resistance is directly proportional to the membrane thickness. Thus, a higher pressure potential is required to obtain similar

absorption rates for the case of the membrane with 0.45 μm pore diameter and greater thickness.

In the membrane absorption process, an increase in the pressure potential is followed by an increase in the absorption rate. The effect of the pressure potential is represented in Fig. 10 by means of the absorption ratio. This ratio is defined as the rate of vapour absorbed normalized to the solution flow rate. In this way, the effect of the differences in solution mass flow rates in the experiments is subtracted: for given solution mass flow rates, high absorption rates are equivalent to high absorption ratios. As expected, the absorption ratio increases with the pressure potential for the three membranes, with a linear rate of change equal to 0.04 (kg_v/kg_s) per kPa.

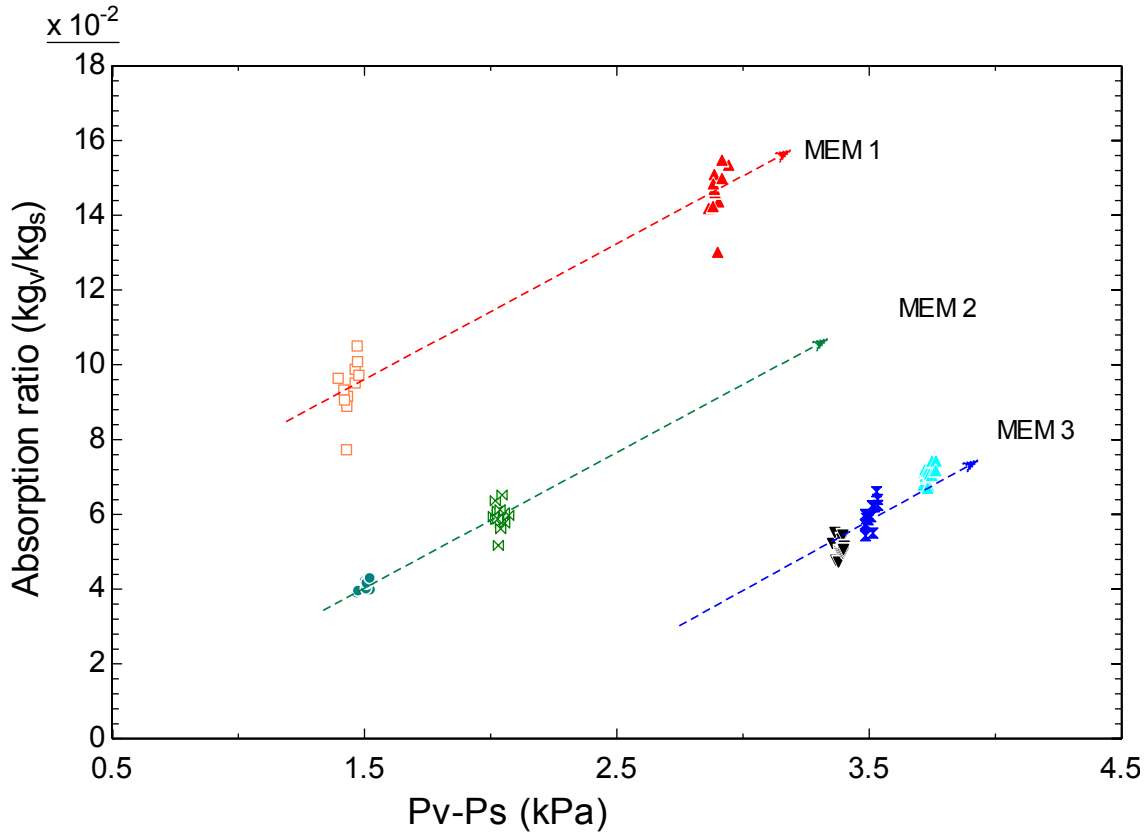

Fig. 10. Ratio of water vapour absorbed to solution mass rates for the three membranes tested.

Previous works in adiabatic absorbers using atomizers to obtain solution flat sheets or sprays to increase the mass transfer between the vapour and the solution used this same parameter to characterize the performance of the absorber. The absorption ratios (from 0.04 to 0. 16 kg_v/kg_s) in our experiments were higher than the ones of Palacios et al. [22], who obtained ratios lower than 0.016 kg_v/kg_s. Warnakulasuriya and Worek [23]

reached 0.0055 kg_v/kg_s but using H_2O-LZB^{TM}. The configurations of these absorbers were based on cylindrical chambers. The advantage of the present configuration is that the performance can be maintained by increasing the number of modules, as observed by Schwerdt [14].

As previously discussed, in the case of the membranes with 0.45 μm pore diameter, but different membrane thickness (MEM2 and MEM3), the higher thickness increases the pressure potential required to obtain a similar performance. According to the theoretical study of Ali and Schwerdt [1], an increase of the membrane thickness from 50 to 127 μm in a membrane with a pore diameter of 0.45 μm, reduces the absorption rate by 55%. The model of Venegas et al. [9] gives, for the same change in thickness, a 45% decrease.

The higher pore diameter induces a higher absorption rate for a given pressure potential. The membrane with 1 μm pore diameter has a lower porosity (higher tortuosity) and a larger thickness. The reduction in pore size from 1 to 0.45 μm, according to Ali and Schwerdt [1] will decrease the absorption rate by 50% (for similar thickness and porosity).

In order to estimate the agreement between those previous models and our results, we plot in Fig. 11 the values of the absorption ratio actually measured for the case of 1 μm pore diameter and 175 μm thickness (MEM1). In the same figure, the results shown for the cases of MEM2 and MEM3 are derived from the measured ones, but applying the correction factors obtained from Fig. 9 and Fig. 10 of Ali and Schwerdt [1]. Fig. 9 of that study provides the factor of change in absorption rate due to thickness and pore diameter while Fig. 10 is used to obtain the correction factor to take into account the differences in porosity. For each measured condition, these factors are normalized with the solution mass flow rate, as we consider the absorption ratio.

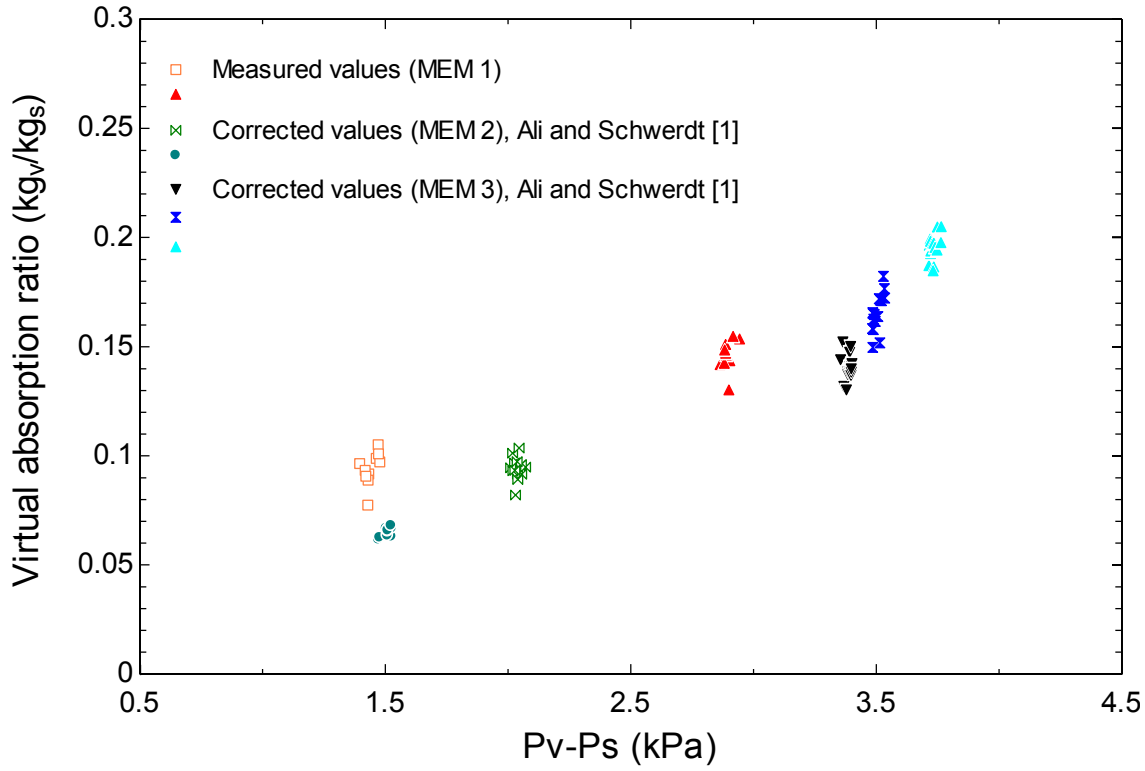

Fig. 11. Virtual ratio of water vapour absorbed to solution mass rates obtained with the corrections factors of previous models for a unique membrane of 1 μm pore diameter and 175 μm thickness.

It is seen that these virtual changes in the membrane properties provide a reasonable behaviour for the entire range of pressure potentials and solution mass flow rates studied for a virtual membrane of 1 μm and 175 μm.

The overall mass transfer resistance calculated from the experimentally obtained absorption rate and pressure potential is:

$$R_{OV} = \frac{P_v - P_s}{J} \tag{2}$$

As discussed in previous works (Venegas et. al [8]), the resistance to mass transfer in the vapour phase is negligible and therefore R_{OV} takes into account the resistance through the solution boundary layer (R_s) and the resistance through the membrane (R_m).

The mass transfer mechanism through the membrane depends on the Knudsen number. During our experiments, the calculated Knudsen number determined that the membrane was working in the transition flow regime. Therefore, the mass transport resistance of the membrane is the result of two parallel resistances one due to the contribution of the Knudsen flow and the other to the Poiseuille flow:

$$\frac{1}{R_m} = \frac{M}{e_m}\left(\frac{D_e}{R_u T_m} + \frac{P_m B_0}{R_u T_m \mu_v}\right) \tag{3}$$

where:

$$D_e = \frac{\varepsilon d_p}{3\tau}\left(\frac{8R_u T_m}{\pi M}\right)^{0.5} \quad (4)$$

$$B_0 = \frac{\varepsilon d_p^2}{32\tau} \quad (5)$$

In Eqs. (3) and (4), M is the water molecular weight, R_u is the universal gas constant, T_m is the membrane temperature and μ_v refers to the vapor viscosity. In Eqs. (4) and (5), ε is the porosity and τ the tortuosity of the membrane. Tortuosity was calculated using the expression provided by Iversen et al. [24]:

$$\tau = \frac{(2-\varepsilon)^2}{\varepsilon} \quad (6)$$

In the previous expressions, the water and solution properties were obtained from the literature (Patek and Klomfar [25], Harr et al. [26], Lee et al. [27], DiGuilio et al. [28] and the Electrical Research Association [29]).

The mass transfer resistance of the bulk solution can be calculated as the difference between the derived overall resistance obtained from the measurements as in Eq. (2) and the calculated resistance to vapour flow of the membrane obtained as in Eq. (3):

$$R_s = R_{OV} - R_m \quad (7)$$

The mean values of both resistances (R_m and R_s) are represented in Fig. 12 for each membrane and operating conditions.

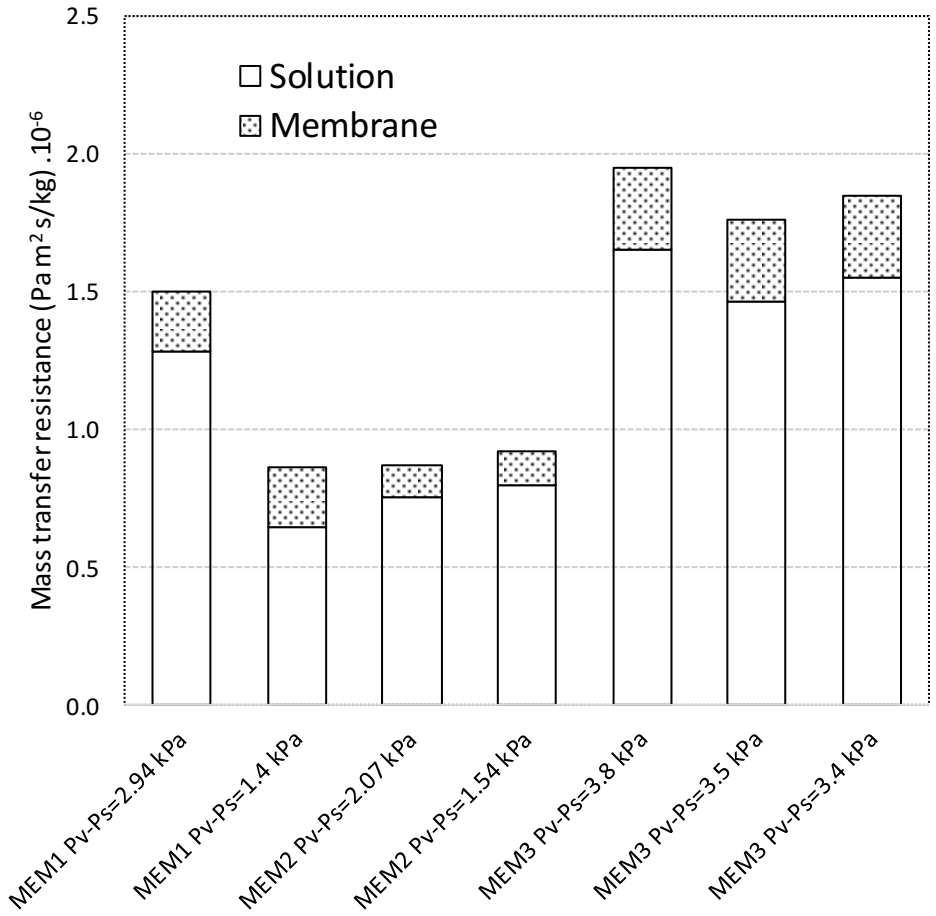

Fig. 12. Mass transfer resistances (membrane and solution) for each experimental case.

The higher membrane resistance corresponds to the lower diameter pore and higher thickness (MEM3). The membrane with pore diameter 0.45 μm and lower thickness (MEM2) presents the lower membrane resistance. The combination of a high pore diameter (1 μm) and a high thickness and lower porosity, provides a membrane with a mass transfer resistance that is higher than a lower pore diameter with a low thickness. This is in accordance with the work of Ali and Schwerdt [1]. The membrane resistance represents in the order of 16% of the overall mass transfer resistance, as in Isfahani et al. [11]. This is due to the combination of the channel width and pore diameters of the membranes. Therefore, the variation of the overall resistance with the different experimental conditions is attributed to the bulk mass transfer resistance. The dependence with mass flow rate of this last one (the solution mass transfer resistance) is represented in Fig. 13.

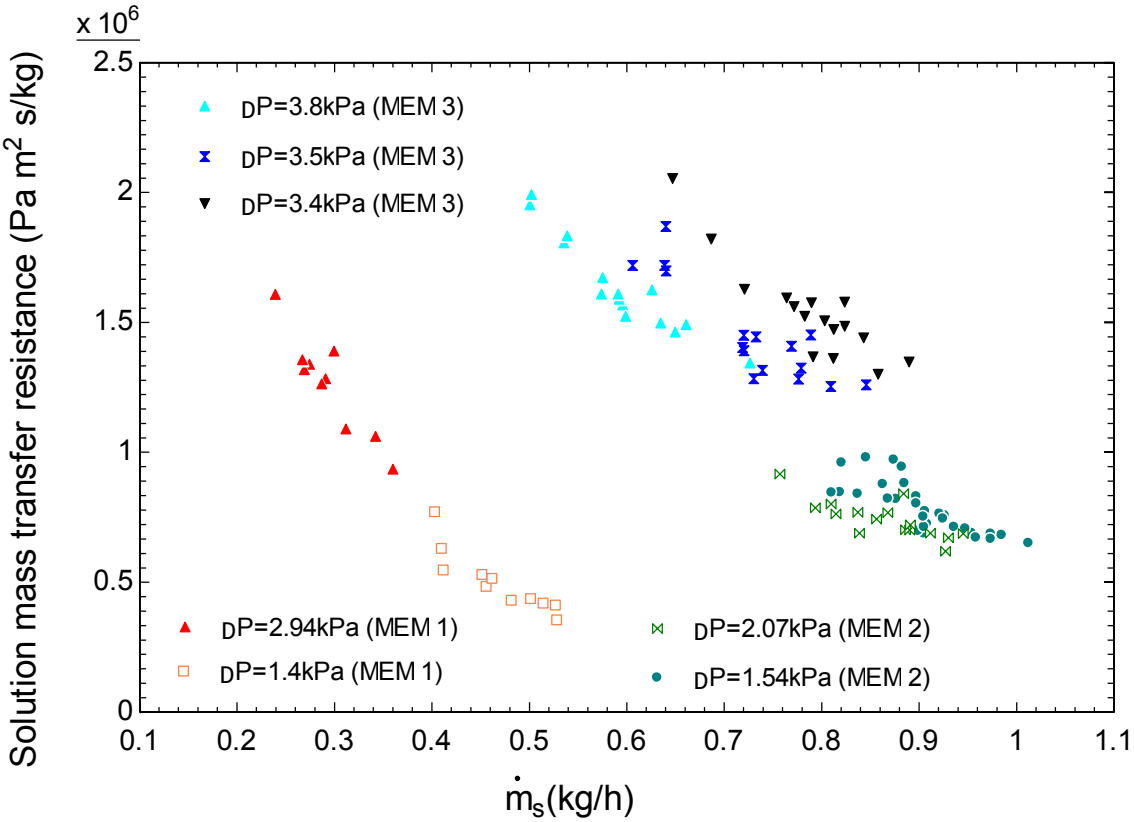

Fig. 13. Solution mass transfer resistance.

There is a decrease in the mass transfer resistance, as indicated by Isfahani et al. [12] and Venegas et al. [9] with the solution mass flow rate. As the mass transfer resistance is obtained by normalizing the absorption rate with the pressure potential, the dependance with the pressure potential appears to be less pronounced.

The solution mass transfer resistance has been calculated in previous models of membrane absorbers as:

$$R_s = \frac{P_{sat}}{\rho_w k_s} \tag{8}$$

where P_{sat} is the saturated water pressure at the bulk solution temperature, ρ_w is the water density and k_s is the mass transfer coefficient in the aqueous solution boundary layer.

Mass transfer coefficients can be correlated using expressions of the form:

$$\frac{k_S D_h}{D} = Sh \propto Re^a \, Sc^b f(geometry) \tag{9}$$

where Sh is the Sherwood number, Re, the Reynolds number and Sc, the Schmidt number. D_h corresponds to the hydraulic diameter of the channels and D is the diffusion coefficient.

Ali [2] employed the correlation of Gabelman and Hwang [30] to calculate k_s in Eq. (9). Venegas et al. [8] used instead the heat and mass transfer analogy and used correlations of Lee and Garimella [31] and Shah and London [32]. In both cases, the dependence of the coefficient k_s is parabolic, similar to the tendency shown in the experiments in Fig. 13.

In Fig. 14 we represent the mean values, for each of the membranes and operating pressure potentials, of the overall mass transfer resistance calculated as the sum of the calculated membrane resistance R_m and the calculated R_S, as in Eq. (8), using the correlation proposed by Ali [2] and the correlation of Venegas et al. [8]. In the figure, the predicted values are compared to the mean experimental values. The standard deviation of the experimental overall mass transfer resistances is also plotted.

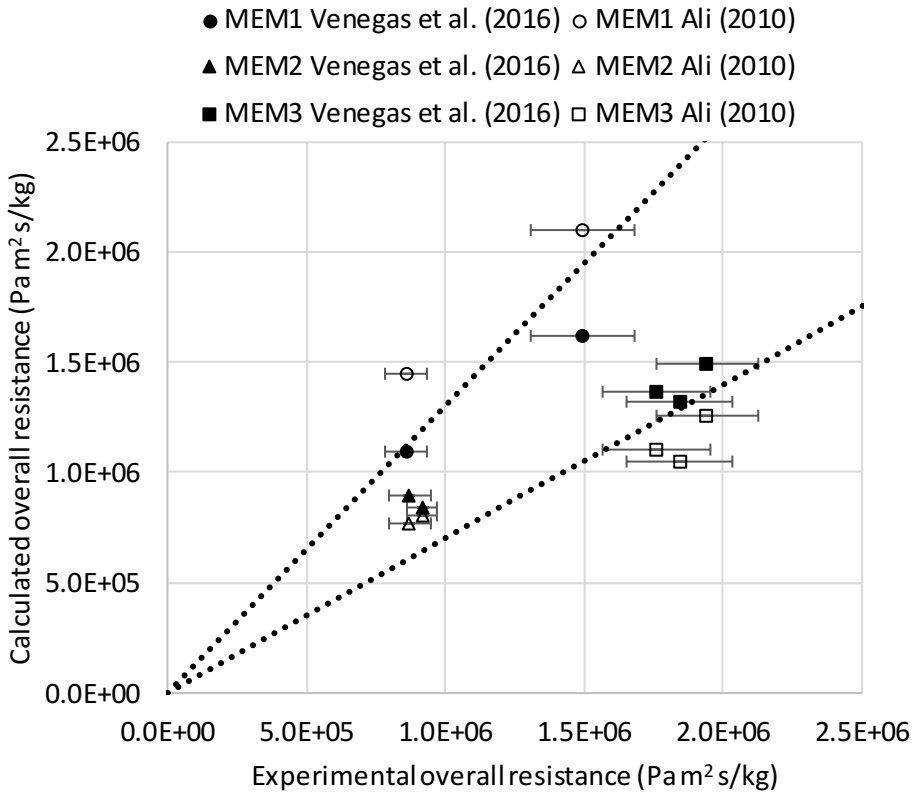

Fig. 14. Mean experimental and calculated overall mass transfer resistances.

Differences between experiments and the model of Venegas et al. [10] are below 30%. The correlation proposed by Ali [2] to calculate R_S, in this case, has higher errors. The original correlation of Gabelman and Hwang [30] was derived for hollow fiber membrane contactors, while the heat transfer correlations employed in Venegas et al. [8] were originally developed for rectangular channels, as the ones in our experiments.

5. Conclusions

The objective of this study was to experimentally measure the water vapour mass flux absorbed in a H_2O-LiBr solution, using a microchannel adiabatic absorber operating with three different flat PTFE membranes. The effect of the change in pore diameter and thickness on the absorber performance follows the tendencies predicted in previous theoretical studies. The absorption rate increases with the solution mass flow rate and the pressure potential, with values that range from 1.5 10^{-3} to 2.6 10^{-3} kg/m^{2}s. These values are lower than the ones obtained with cooled absorbers. Nevertheless, with this configuration, construction can be easier, with the possibility of using non-conductive materials, which can make the construction commercially simple. The 1 μm pore diameter membrane provides higher absorption rates at low solution mass flow rates. The absorption ratios obtained for the three membranes are higher than the ones found in previous works using cylindrical adiabatic absorbers working with water as the refrigerant. The advantage of the present design and its modular implementation is that the absorption rate can be scaled up on demand. Increasing the number of channels, or overlapping modules as the one presented, without changing the conditions of the absorption process, are ways to easily increase the quantity of vapour absorbed.

The reduction of the pore diameter from 1 μm to 0.45 μm requires a doubling of the solution mass flow rate to maintain the same absorption rate. The difference in thickness from 25-51 to 76-127 μm, for a given mass flow rate, leads to operation with a doubled pressure potential to obtain a similar absorption rate. These results are similar to the ones predicted in previous models. To check this conclusion, two virtual membranes have been compared to the one of 1 μm pore diameter and 175 μm thickness by applying the correction factors provided by those models to the experimental results.

The size of the membrane pore diameter and the fact that the channels used are 150 μm height, imply that the solution mass transfer governs the mass transfer process. The measured film solution resistance follows a power law decrease with mass flow rate as suggested by previous theoretical studies. The experimental values of the overall mass transfer resistance, compared to the calculated ones using previous correlations found in the literature, agree within differences below 30%.

Acknowledgements

Financed by: FEDER/Ministerio de Ciencia, Innovación y Universidades – Agencia Estatal de Investigación/ Project (DPI2017-83123-R).

References

[1] Ali AHH, Schwerdt P. Characteristics of the membrane utilized in a compact absorber for lithium bromide-water absorption chillers. Int J Refrig 2009;32:1886–96.

[2] Ali AHH. Design of a compact absorber with a hydrophobic membrane contactor at the liquid-vapor interface for lithium bromide-water absorption chillers. Appl. Energy 2010;87:1112–21.

[3] Yu D, Chung J, Moghaddam S. Parametric study of water vapour absorption into a constrained thin film of lithium bromide solution. Int J Heat Mass Transf 2012;55:5687–95.

[4] Bigham S, Yu D, Chugh D, Moghaddam S. Moving beyond the limits of mass transport in liquid absorbent microfilms through the implementation of surface-induced vortices. Energy 2014;65:621–30.

[5] Asfand F, Stiriba Y, Bourouis M. CFD simulation to investigate heat and mass transfer processes in a membrane-based absorber for water-LiBr absorption cooling systems. Energy 2015;91:517–30.

[6] Asfand F, Stiriba Y, Bourouis M. Performance evaluation of membrane-based absorbers employing H_2O/(LiBr + LiI + $LiNO_3$ + LiCl) and H_2O/($LiNO_3$ + KNO_3 + $NaNO_3$) as working pairs in absorption cooling systems. Energy 2016;115:781–90.

[7] Asfand F, Stiriba Y, Bourouis M. Impact of the solution channel thickness while investigating the effect of membrane characteristics and operating conditions on the performance of water-LiBr membrane-based absorbers. Appl Therm Eng 2016;108:866–77.

[8] Venegas M, de Vega M, García-Hernando N, Ruiz-Rivas U. A simple model to predict the performance of H_2O-LiBr absorber operating with a microporous membrane. Energy 2016;96:383–93.

[9] Venegas M, de Vega M, García-Hernando N. Parametric study of operating and design variables on the performance of a membrane-based absorber, Appl Therm Eng 2016;98:409–19.

[10] Venegas M, de Vega M, García-Hernando N, Ruiz-Rivas U. Adiabatic vs non-adiabatic membrane-based rectangular microabsorbers for H_2O-LiBr absorption chillers. Energy 2017;134:757–66.

[11] Isfahani RN, Moghaddam S. Absorption characteristics of lithium bromide (LiBr) solution constrained by superhydrophobic nanofibrous structures. Int J Heat Mass Transf 2013;63:82–90.

[12] Isfahani RN, Sampath K, Moghaddam S. Nanofibrous membrane-based absorption refrigeration system. Int J Refrig 2013;36:2297–307.

[13] Isfahani RN, Bigham S, Mortazi M, Wei X, Moghaddam S. Impact of micromixing on performance of a membrane-based absorber. Energy 2015 90: 997-1004.

[14] Schwerdt P. Activities in thermal driven cooling at Fraunhofer Umsicht. In: Thermally driven heat pumps for heating and cooling. Ed. Annett Kühn. Universitätsverlag der TU Berlin, 2013:117–26.

[15] García-Hernando N, de Vega M, Venegas M. Experimental characterisation of a novel adiabatic membrane-based micro-absorber using H2O-LiBr. Int.J. Heat and Mass Tranf 2019;129:1136-43.

[16] Wang P, Chung T-S. Recent advances in membrane distillation processes: Membrane development, configuration design and application exploring. J Membr Sci 2015;474:39-56.

[17] http://www.merckmillipore.com/ES/es/product/Fluoropore-Membrane-PTFE-hydrophobic-1.0m-293mm-white-plain,MM_NF-FALP29325 Last accessed 7 september 2018

[18] https://www.sterlitech.com/ptfe-unlaminated-membrane-filter-ptu0453001.html Last accessed 7 september 2018

[19] https://www.sterlitech.com/ptfe-laminated-membrane-filter-ptfe0453005.html Last accessed 7 september 2018

[20] Hong SJ, Taira N., Hihara E., Dang C. Opportunity and challenge of developing hydrophobic membrane-based compact absorption system. 12th IEA Heat Pump Conference 2017. Rotterdam.

[21] Taylor BN, Kuyatt CE. Guidelines for evaluating and expressing the uncertainty of NIST measurement results, National Institute of Standards and Technology, NIST technical note 1297, 1994

[22] Palacios E, Izquierdo M, Marcos JD, Lizarte R. Evaluation of mass absorption in LiBr flat-fan sheets, Appl Energy 2009;86:2574–82.

[23] Warnakulasuriya FSK, Worek WM. Adiabatic water absorption properties of an aqueous absorbent at very low pressures in a spray absorber, Int J Heat Mass Transf 2006;49:1592–602.

[24] Iversen SB, Bhatia VK, Dam-Johansen K, Jonsson G. Characterization of microporous membranes for use in membrane contactors, J Membr Sci 1997;130:205–17.

[25] Patek J, Klomfar J. A computationally effective formulation of the thermodynamic properties of LiBr-H2O from 273 to 500 K over full composition range, Int J Refrig 2006;29:566–78.

[26] Harr L, Gallagher JS, Kell GS. NBS/NRC steam tables. Hemisphere Publishing Co., New York, 1984.

[27] Lee RJ, DiGuilio RM, Jeter SM, Teja AS. Properties of lithium bromide-water solutions at high temperatures and concentrations - II density and viscosity, ASHRAE Trans 1990;RP-527:709–14.

[28] DiGuilio RM, Lee RJ, Jeter SM, Teja AS. Properties of lithium bromide-water solutions at high temperatures and concentrations - I thermal conductivity, ASHRAE Trans 1990;RP-527:702–8.

[29] Electrical Research Association Steam Tables, Thermodynamic properties of water and steam; viscosity of water and steam, thermal conductivity of water and steam, Edward Arnold Publishers, London, 1967.

[30] Gabelman A, Hwang S-T. Hollow fibre membrane contactors, J Membr Sci 1999;159:61-106.

[31] Lee P-S, Garimella SV. Thermally developing flow and heat transfer in rectangular microchannels of different aspect ratios. Int J Heat Mass Transf 2006;49:3060-7.

[32] Shah RK, London AL. Laminar flow forced convection in ducts. In: A source book for compact heat exchanger analytical data. Advances in heat transfer. NewYork: Academic Press; 1978. Suppl. 1.